Journal of Solid State Chemistry **145,** 110–115 (1999)
Article ID jssc.1999.8229, available online at http://www.idealibrary.com on IDEAL®

# X-Ray and Ultraviolet Luminescence of $Li_3Ta_{1-x}Nb_xO_4$ Prepared by Flux Synthesis and Characterization of a New High Efficiency X-Ray Phosphor

C. R. Miao and C. C. Torardi

*DuPont Company, Central Research and Development, Experimental Station, Wilmington, Delaware 19880-0356*

Received November 25, 1998; in revised form February 2, 1999; accepted February 15, 1999

**The phase development and luminescence properties, under both X-ray and ultraviolet excitation, of the lithium orthotantalate–lithium orthoniobate system, $Li_3Ta_{1-x}Nb_xO_4$ for $x = 0$ to 1, were examined. Using a flux synthesis technique, it was found that the levels of Nb-doping in monoclinic $Li_3TaO_4$ and of Ta-doping in cubic $Li_3NbO_4$ are higher than previously reported. Under 30 kVp molybdenum X-ray excitation, $Li_3Ta_{1-x}Nb_4O_4$ is an efficient blue-emitting phosphor with broadband emission, peaking in the range of 390 to 435 nm. For $x = 0$ to 0.1, the overall luminescence efficiency is comparable to, or better than, a commercial calcium tungstate, $CaWO_4$, Hi-Plus material. The composition $Li_3Ta_{0.995}Nb_{0.005}O_4$ demonstrates an overall luminescence efficiency that makes this phosphor 45% brighter than $CaWO_4$ Hi-Plus, thereby making it a potentially attractive candidate for use in medical diagnostic imaging systems. Under ultraviolet excitation, broadband blue emission is also observed. For all the $Li_3Ta_{1-x}Nb_xO_4$ ($x > 0$) solid solutions, the emission peak maximums agree well with those seen under X-ray excitation and are the result of $Nb^{5+}$ emission.** © 1999 Academic Press

## INTRODUCTION

X-ray phosphors are solid-state inorganic materials used in medical X-ray imaging applications (1, 2). The role of these phosphors is to reduce the exposure of the patient to X-rays while preserving the structural features of the X-ray image. This is accomplished by converting every X-ray photon absorbed by a phosphor screen into hundreds of visible- or UV-light photons which are then recorded by a detector, such as a piece of photographic film. A good X-ray phosphor must meet challenging prerequisites (1–3): good X-ray absorption in the diagnostic medical energy range (15–100 keV), high luminescence efficiency, emission in the green to near-UV region, proper crystallite size and shape, air and water stability, and easy large-scale production. The goal of our X-ray phosphor research was to design materials that would lower X-ray exposure and improve image quality.

In this paper, we describe the flux synthesis, structural phase transitions, and luminescence of an efficient X-ray phosphor family $Li_3Ta_{1-x}Nb_xO_4$ ($x = 0$–1). Prior to this work, the two end-member compositions had been prepared using traditional solid-state methods (4, 5) and only a brief examination of their UV-excited luminescence properties had been performed (5). This paper focuses on the characterization of the luminescence properties of the entire range of compositions under both X-ray and UV-excitation. We report the optimum chemical composition region ($x \sim$ 0.001–0.01) that results in blue, broadband X-ray excited luminescence, peaking at $\sim$ 415 nm, with intensity greater than that of $CaWO_4$ Hi-Plus and comparable to that of M′-$YTa_{0.98}Nb_{0.02}O_4$, a very successful commercial phosphor (6).

## EXPERIMENTAL

### *Synthesis*

Stoichiometric quantities of $Li_2CO_3$ (J. T. Baker reagent grade, 99.6%), $Ta_2O_5$ (Stark standard optical grade, 99.96%), and $Nb_2O_5$ (Johnson–Matthey puratronic, 99.998%) were combined according to the equation

$$3\ Li_2CO_3 + (1 - x)\ Ta_2O_5 + x\ Nb_2O_5 \rightarrow 2\ Li_3Ta_{1-x}Nb_xO_4 + 3\ CO_2$$

and mixed with $Li_2SO_4$ flux. The amount of $Li_2SO_4$ was equal to 35% of the combined weights of the other starting materials. $Li_2CO_3$ is required for the reaction because, in this temperature range, we find that $Ta_2O_5$ will react with $Li_2SO_4$ to form $LiTaO_3$, but not $Li_3TaO_4$. Each sample was ground in an agate mortar, fired in a covered alumina crucible at 1000°C for 16 hours, and then furnace cooled. The $Li_2SO_4$ was washed out with water and the sample dried under infrared lamps. X-ray powder diffraction (Phillips APD3720 with Cu radiation) was used to verify phase



0022-4596/99 $30.00

purity. Some preparations contained a very small amount of $LiTaO_3$. These levels of $LiTaO_3$ did not appear to affect the luminescence speed (i.e., efficiency).

### *Physical Characterization*

Particle size analyses were conducted by dispersing the powders in a 70:30 glycerol:distilled water solution using a Sonicator W-375. The resultant dispersion was examined using a Horiba LA-500 laser diffraction particle size distribution analyzer. The particle size, crystallite size, and morphology were also examined using scanning electron microscopy techniques.

### *X-ray Luminescence Measurements*

For measurements of X-ray stimulated luminescence properties, the powders were first mixed with a polymeric binder and coated on a sheet of base material. This technique for making a phosphor "screen" is similar to that used in commercial production (7), and permits the preparation of a screen with a uniform thickness of uniformly dense material. The base material and polymeric binder were chosen to avoid interference with the X-ray luminescence measurements.

The X-ray luminescence of the samples was examined under ambient conditions using a molybdenum X-ray source operating at 30 kVp and 10 mA. The sample was exposed to polychromatic X-radiation, and two detectors were used to measure the luminescence properties (2). The first detection system consisted of a Hamamatsu R928 photomultiplier and a picoammeter and was used to measure the total intensity of light coming from the sample or the overall X-ray-to-light conversion efficiency. The second detection system used a SPEX 500M spectrometer, in which the light from the sample passes through a 0.5-meter monochromator before entering a Hamamatsu R928 photomultiplier. Using this detection system, a characteristic spectrum of the luminescence of the sample could be obtained by scanning through the range of detectable wavelengths allowed by the monochromator and measuring the intensity of light at each interval. The Hamamatsu photomultipliers were selected because of their relatively flat response in the region 300–600 nm.

### *Ultraviolet Luminescence Measurements*

Powder samples were packed into aluminum holders and examined under ultraviolet excitation at room temperature using a SPEX 1680 Fluorolog II double spectrometer which incorporated two 0.22-meter monochromators for monitoring of the excitation and emission spectra. The light from the UV lamp passes through a monochromator, monitored by a Hamamatsu R928 photomultiplier tube, to measure the wavelength and intensity of the energy used to excite the sample. A second monochromator and Hamamatsu R928 photomultiplier tube was used to monitor the light emitted by the sample in much the same way as described above for X-ray luminescence. By holding the excitation energy at a fixed wavelength, an emission spectrum of the sample was obtained. Conversely, an excitation spectrum could also be determined for a fixed emission wavelength.

## RESULTS AND DISCUSSION

### *Structure*

The structure of $Li_3TaO_4$ was initially described as pseudo-tetragonal, with $a = 6.01$ Å and $c = 16.67$ Å (8), but subsequent studies found that there are three different possible forms (9). However, it is the low-temperature pseudo-tetragonal phase, stable below about 900°C, that is discussed in this paper. It exists in a NaCl-type structure in which the cations and anions are octahedrally coordinated. Closer examination, by powder neutron diffraction (4), revealed that the $Li^+$ and $Ta^{5+}$ ions are ordered along the *c*-axis of a pseudo-tetragonal cell with a Ta-Li-Li-Li-Ta repeat sequence, and the structure is best described as monoclinic ($a = 8.50$ Å, $b = 8.50$ Å, $c = 9.34$ Å and $\beta = 117.05°$). The cation ordering creates chains of edge-sharing $TaO_6$ octahedra oriented parallel with the *c*-axis (Fig. 1). The oxygen octahedra of the $TaO_6$ units are distorted, and the *cis*-edge-shared oxygen–oxygen distances are significantly shorter than the remaining O–O contacts. The other forms of $Li_3TaO_4$ were not examined in this work.

Although the structure of $Li_3NbO_4$ contains $NbO_6$ and $LiO_6$ octahedra, it is very different from the tantalate and consists of isolated edge-sharing $Nb_4O_{16}$ clusters interconnected by $LiO_6$ units (10).

### *Synthesis and Characterization*

The synthesis of the low-temperature form of $Li_3TaO_4$ by conventional solid-state techniques, used by Zocchi *et al.* (4), involves reacting lithium metatantalate and lithium carbonate. Following their procedure, $LiTaO_3$ and $Li_2CO_3$ were ground together and heated for 20 hours at 700°C, reground and heated for 120 hours at 800°C, and then reground and heated for 17 hours at 1000°C to obtain phase pure material.

We have discussed the benefits of using flux techniques to synthesize phosphor materials (2, 11), in particular, the important X-ray phosphor M′-$YTaO_4$ (6, 11). By employing a $Li_2SO_4$ flux to facilitate the reaction between $Li_2CO_3$ and $Ta_2O_5$, it was found that the reaction time for the synthesis of $Li_3TaO_4$ could be reduced by a factor of ten. Particle size measurements showed that the flux synthesized powders contained considerably larger particles than those obtained from the solid-state method. The median particle size of the

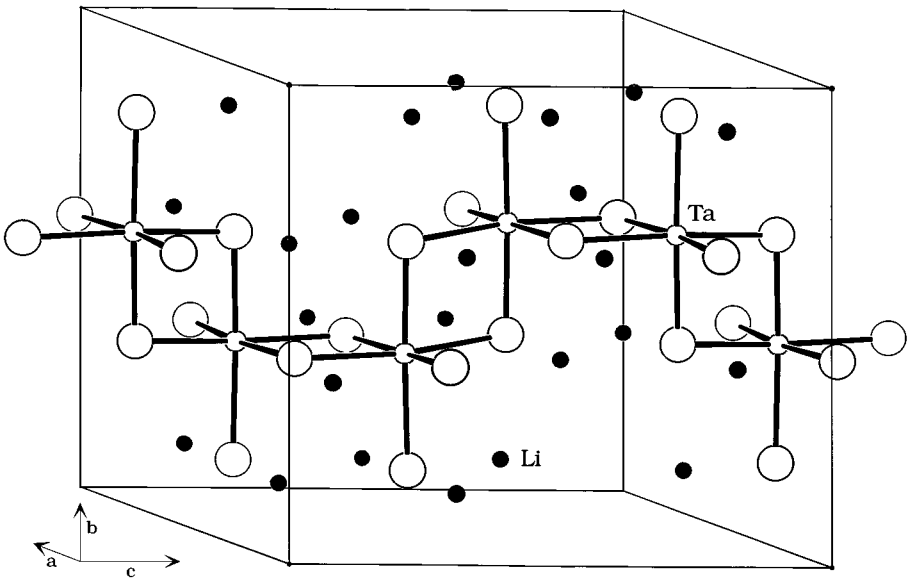


**FIG. 1.** Monoclinic structure of $Li_3TaO_4$ emphasizing edge-sharing of $TaO_6$ octahedra. Li atoms are shaded. For clarity, Li–O bonds are not shown.

former, using a $Li_2SO_4$ flux, was 34 μm, while the latter yielded a median size of 7.5 μm.

Using scanning electron microscopy, it was found that the powders formed by solid-state synthesis were comprised of approximately 3 to 15 μm agglomerates that consisted of 1 to 3 μm crystallites fused together in porous networks. It is likely that this morphology arises from partial melting of the crystallites during the synthesis. It would be expected that this combination of small crystallite size and porous morphology would lead to a decrease in luminescence efficiency. The small crystallites, and consequently high surface area, would reduce the bulk emission, and the porous network of particles would reduce the packing density of the phosphor.

In comparison, the powders of $Li_3TaO_4$ obtained from flux synthesis displayed a more isotropic polyhedral shape which could provide more efficient packing in a phosphor screen. Although the larger size of the crystallites, which were approximately 10 to 70 μm, may present difficulties in coating thin screens, in previous studies of the related M′-$YTaO_4$ system this problem was overcome through the utilization of finer starting materials, post-reaction milling, or adjustments of the reaction time and temperature and amount of flux. These variations were not explored for $Li_3TaO_4$ in this work.

The crystallites of $Li_3NbO_4$ formed by flux synthesis were smaller than those prepared for $Li_3TaO_4$ and had a less uniform size distribution (0.5 to 20 μm).

The flux method was also utilized to explore the solubility of Nb in monoclinic $Li_3TaO_4$. Previous studies of solid-solution formation in the $Li_3Ta_{1-x}Nb_xO_4$ system had employed solid-state preparative methods (12). This work showed that up to 20% Nb could be substituted for Ta in $Li_3TaO_4$ and that solubility of Ta in $Li_3NbO_4$ was very limited (about 7%). By examining compositions across the entire system, it was found that the flux method significantly increases the degree of solid solubility under the synthesis conditions described above. For example, an X-ray powder diffraction pattern collected from a sample of monoclinic $Li_3Ta_{1-x}Nb_xO_4$ with $x = 0.6$ could be indexed in terms of a single phase product. The use of a flux also extended the solubility of Ta in cubic $Li_3NbO_4$ up to approximately 20% Ta replacing Nb. Between these two limits, $x = 0.6$ to 0.8, a two-phase mixture of monoclinic $Li_3TaO_4$ and cubic $Li_3NbO_4$ was formed.

### *X-ray Luminescence*

The X-ray excited luminescence of flux-derived samples of $Li_3TaO_4$ is shown in Fig. 2. The spectrum is similar to that of M′-$YTaO_4$ (6), with a broadband due to self-activated $Ta^{5+}$ emission. The shift to a slightly longer wavelength (395 nm vs 330 nm for M′-$YTaO_4$) is likely due in part to the presence of the lithium octahedra. Whereas in M′-$YTaO_4$ there is one yttrium ion in eight-fold coordination with oxygen for every $TaO_6$ unit, $Li_3TaO_4$ has three lithium octahedra for each $TaO_6$ unit. This leads to stronger vibronic coupling between the lattice and each luminescent center and consequently a slightly larger Stokes shift (the optical absorption edges for both compounds are approximately equal (13)). It is perhaps significant that $Li_3TaO_4$ has edge-sharing chains of $TaO_6$ octahedra (Fig. 1), a structural feature found in $YTaO_4$-type phosphors (2). The effect of bringing together highly charged $Ta^{5+}$ ions in parallel

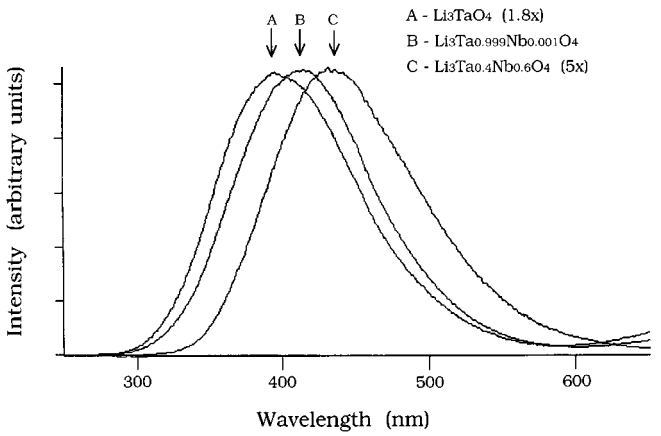


**FIG. 2.** Broadband blue emission of $Li_3Ta_{1-x}Nb_xO_4$ for $x = 0$ (395 nm), $x = 0.001$ (410 nm), and $x = 0.60$ (435 nm) under X-ray excitation (Mo, 30 kVp). Intensities for the $x = 0$ and 0.60 spectra are scaled.

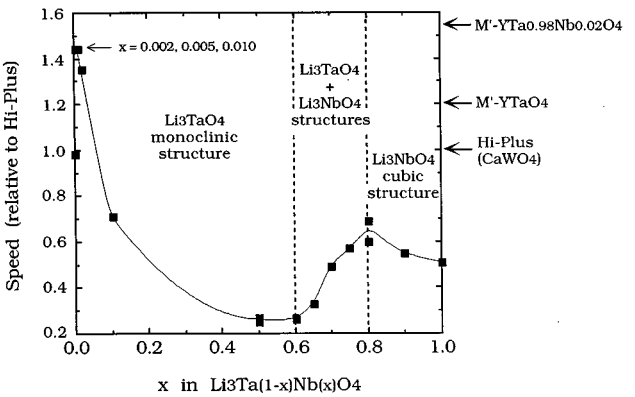


**FIG. 4.** Luminescence efficiency (speed) of X-ray excited $Li_3Ta_{1-x}Nb_xO_4$. Speed values are relative to a $CaWO_4$ Hi-Plus standard. Relative speeds of M′-$YTaO_4$-type phosphors are also compared.

chains throughout the structure may be an important factor in the luminescence of these materials. Because their luminescence is best described as a self-activated charge-transfer mechanism, it is possible that a shorter distance between the luminescent $Ta^{5+}$ cations facilitates energy transfer from the oxygen ligands and encourages significant electronic reorganization.

As with M′-$YTaO_4$, the substitution of very small levels of niobium results in a shift in the emission peak to the characteristic broad blue peak of niobium, at approximately 410 nm for $x = 0.001$ in $Li_3Ta_{1-x}Nb_xO_4$ (Figs. 2 and 3). In these materials, some of the tantalum emission is lost to niobium, since the large amount of spectral overlap between the two ions results in a high rate of energy transfer.

As the level of Nb-doping in $Li_3TaO_4$ is increased, the peak maximum of the emission gradually shifts to lower energy, up to approximately 435 nm for $x = 0.6$ (Figs. 2 and 3). This increase in the Stokes shift is attributable to an increase in the vibronic coupling of the lattice. The fact that $Li_3NbO_4$ does not form a monoclinic phase similar to that of $Li_3TaO_4$ implies that the $Nb^{5+}$ ion is not generally stable in the octahedral coordination of the $Ta^{5+}$ ion found in $Li_3TaO_4$. Therefore, substituting Nb into $Li_3TaO_4$ introduces a great deal of strain on the lattice, and strong vibronic coupling with the $Nb^{5+}$ defect centers is required to maintain the structure.

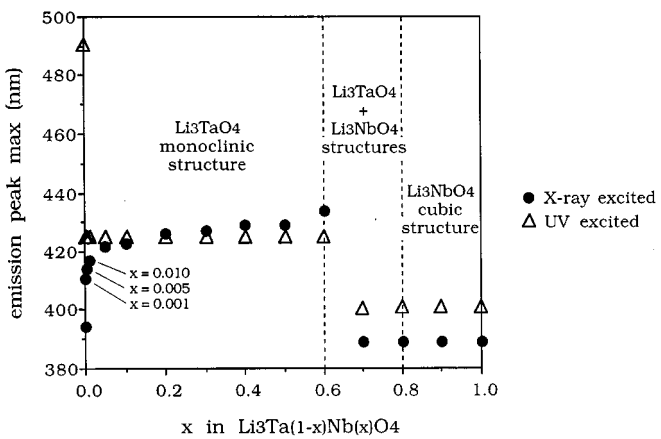


**FIG. 3.** Change in X-ray and UV excited emission peak maximum with $x$ in $Li_3Ta_{1-x}Nb_xO_4$.

Figure 4 shows the overall luminescence efficiency, or speed, of undoped $Li_3TaO_4$ and Nb-doped $Li_3TaO_4$ relative to a calcium tungstate Hi-Plus standard. The undoped material displays a speed comparable to that of $CaWO_4$ (various flux preparations of $Li_3TaO_4$ had speeds in the range of $\sim 0.7$–1.0 relative to Hi-Plus). However, the maximum luminescence efficiency is observed at $x \sim 0.005$ (i.e., in the composition region $x = 0.001$–0.010), with a speed approximately 45% greater than that of Hi-Plus (7). This relative overall brightness is greater than that of commercial UV-emitting M′-$YTaO_4$ and approaches that of blue-emitting Nb-doped M′-$YTaO_4$ (1, 2, 6). However, Nb-doped $Li_3TaO_4$ is not an ultraviolet emitter and it has lower X-ray absorption than M′-$YTaO_4$ (it has approximately 75% of the density of $YTaO_4$, 5.75 vs 7.58 g/cm$^3$). Nonetheless, a blue-emitting phosphor that is 45% brighter than $CaWO_4$ could be of interest to the X-ray phosphor industry (7).

As can be seen in Fig. 4, the luminescence efficiency of Nb-doped $Li_3TaO_4$ rapidly declines as increasing amounts of niobium are added. The rapid quenching of the overall luminescence of these samples may be attributable to the coupling of the $Nb^{5+}$ luminescent centers at the higher substitutional levels.

The luminescence of the two-phase region of the system and of the Ta-doped $Li_3NbO_4$ region were also examined and were found to exhibit luminescence properties similar to $Li_3NbO_4$ (Figs. 3 and 4).

*Ultraviolet Luminescence*

Previous investigations of the ultraviolet-excited luminescence of $Li_3TaO_4$ and $Li_3NbO_4$ (5) indicated that the peak emission energy for the tantalate occurs at a much lower energy (460 nm) than that of the niobate (370 nm). In the experiments conducted here on the flux-grown samples, similar results were obtained, with a weak, broad peak observed at 490 nm for $Li_3TaO_4$ and a much stronger broad peak found at 400 nm for $Li_3NbO_4$. The possibility that the 490-nm luminescence was due to a very small amount of $LiTaO_3$ impurity was eliminated by examining a sample of pure $LiTaO_3$, which showed an even lower intensity emission. The very weak low energy emission of $Li_3TaO_4$ may be attributable to the spectral limitations of available equipment as discussed earlier (5). Typical ultraviolet excitation energies (approximately $\lambda = 250$ nm) are high enough to overcome the band gap in $Li_3NbO_4$ ($\sim$250 nm) but slightly less than that of $Li_3TaO_4$ ($\sim$225 nm). As a result, the UV luminescence from $Li_3TaO_4$ may be of a weak phosphorescence type with significant energy lost in removing trapped electrons from the band gap. For $Li_3NbO_4$, a fairly normal fluorescence would be expected.

As seen with the X-ray luminescence measurements, under UV-excitation the addition of Nb in $Li_3TaO_4$ results in a blue emission peak characteristic of $Nb^{5+}$. The weak phosphorescence at 490 nm for undoped $Li_3TaO_4$ becomes a 10-fold stronger 425 nm peak for as little as $x = 0.001$ in $Li_3Ta_{1-x}Nb_xO_4$. The $Nb^{5+}$ ions in the $TaO_6$ octahedra apparently function as isolated luminescent centers, and the emission spectra remain unchanged throughout the monoclinic phase region (Figs. 3 and 5). A shoulder observed on the low energy side of the emission peak present throughout the compositional series is an artifact of the measurement method and arises from a difference in monochromator sensitivity due to a change in gratings. Under UV-excitation, the emission peak maximum lies at approximately the same wavelength as that under X-ray excitation. However, the gradual shift of the peak to lower energy with additional niobium, observed under X-ray excitation, is not observed with UV excitation, indicating that, even at low Nb-doping levels, only the niobium centers can be excited. Also, the rapid decrease in efficiency for $x > 0.01$ under X-ray excitation (Fig. 4) is not seen in our UV study. In fact, qualitative measurements show the UV-excited efficiency rapidly increasing from $x = 0.001$ to 0.10, and maximum efficiency over a wide range, $x \sim 0.2$–0.3, in the monoclinic $Li_3TaO_4$ structure-type region.

Finally, the spectrum of the two-phase mixture, at $x = 0.7$ in $Li_3Ta_{1-x}Nb_xO_4$, as well as the spectra of the samples having the cubic $Li_3NbO_4$ structure, exhibit the characteristic 400-nm niobate emission of $Li_3NbO_4$. This is similar to the results for X-ray excited luminescence and is the result of the $Ta^{5+}$ ions losing all of their excited state energy to the lower energy $Nb^{5+}$ ions.

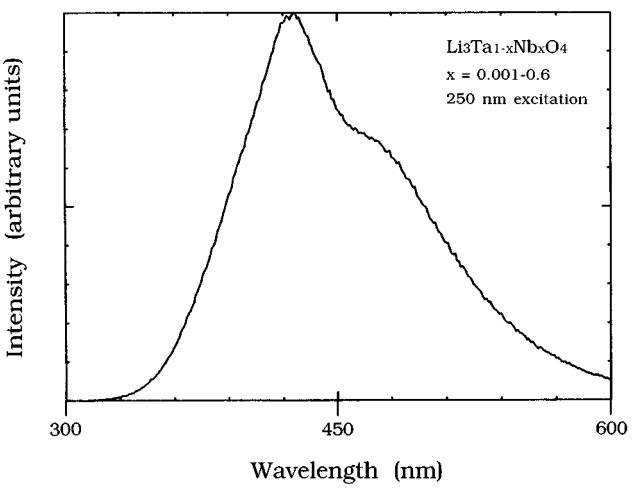


**FIG. 5.** Characteristic emission spectrum of monoclinic $Li_3Ta_{1-x}Nb_xO_4$ for $x$ values of 0.001 to 0.6, peaking in the blue region (425 nm) under 250 nm UV-excitation. (Feature at 450 nm is due to a monochromator grating change.)

## CONCLUSIONS

Lithium orthotantalate, $Li_3TaO_4$, can be easily synthesized using flux chemistry methods. Using a $Li_2SO_4$ flux, the reaction time required to produce phase pure material is greatly reduced compared to a conventional solid-state synthesis procedure. It was found that the use of flux methods also significantly increased the solubility of Nb in $Li_3TaO_4$, allowing 60% Nb to substitute into the monoclinic $Li_3TaO_4$ structure for Ta. The flux methods also extended the solubility of Ta in cubic $Li_3NbO_4$ to 20%.

$Li_3TaO_4$ is an efficient broadband blue-emitting (395 nm) X-ray phosphor with an overall luminescence comparable to $CaWO_4$. Low-level substitution of Nb for Ta improves the luminescence of $Li_3TaO_4$, with peak efficiency at compositions close to $Li_3Ta_{0.995}Nb_{0.005}O_4$. In the composition region of $x \sim 0.001$–0.01, the emission peak is centered at $\sim$415 nm, and the overall luminescence efficiency is 45% brighter than a commercial $CaWO_4$ Hi-Plus material. This shifting of the emission peak to lower energy, with the addition of Nb to $Li_3TaO_4$, is the result of an efficient transfer of the excited-state energy of $Ta^{5+}$ ions to $Nb^{5+}$ ions. As the level of Nb substitution is increased in $Li_3Ta_{1-x}Nb_xO_4$, from $x = 0.001$ to $x = 0.6$, a gradual shifting of the emission peak maximum, to 435 nm for $x = 0.6$, is observed due to increased vibronic coupling with the lattice. Despite its lower density compared to $CaWO_4$, the large improvement in X-ray luminescence efficiency of $Li_3Ta_{1-x}Nb_xO_4$ (with $x \sim 0.001$–0.01) makes it an attractive candidate for applications requiring a blue-emitting phosphor.

Under ultraviolet excitation, broadband blue emission was also observed. For all $Li_3Ta_{1-x}Nb_xO_4$ ($x > 0$) solid solutions, the emission peak maximums agree well with those under X-ray excitation, centered at 425 nm for the compositions having the monoclinic $Li_3TaO_4$ structure and 400 nm for those with the cubic $Li_3NbO_4$ structure. The observed spectra are the result of $Nb^{5+}$ emission. For undoped $Li_3TaO_4$, experimental limitations inhibit a clear understanding of the ultraviolet excited luminescence.

## ACKNOWLEDGMENT

We thank P. K. Davies for discussion and comments on the present work, L. H. Brixner, S. L. Issler, and W. Zegarski for general discussions on phosphor materials, C. M. Foris for X-ray powder diffraction data, and M. K. Crawford and B. D. Jones for assistance with the X-ray and UV excitation spectrometers.

## REFERENCES

1. L. H. Brixner, *Mater. Chem. Phys.* **16,** 253 (1987).
2. S. L. Issler and C. C. Torardi, *J. Alloys Comp.* **229,** 54 (1995).
3. R. C. Ropp, "Luminescence and the Solid State," Elsevier Science, Amsterdam, 1991.
4. M. Zocchi, M. Gatti, A. Santoro, and R. S. Roth, *J. Solid State Chem.* **48,** 420 (1983).
5. G. Blasse and A. Bril, *Z. Physik. Chem. Neue Folge* **57,** 187 (1968).
6. L. H. Brixner and H.-Y. Chen, *J. Electrochem. Soc.* **130,** 2435 (1983).
7. C. C. Torardi, U. S. Patent 5,430,302 (1995).
8. G. Blasse, *Z. Anorg. Allg. Chem.* **331,** 44 (1964).
9. L. C. Martel and R. S. Roth, *Bull. Amer. Ceram. Soc.* **60,** 376 (1981).
10. K. Ukei, H. Suzuki, T. Shishido, and T. Fukuda, *Acta Crystallogr.* C **50,** 655 (1994).
11. D. B. Hedden, C. C. Torardi, and W. Zegarski, *J. Solid State Chem.* **118,** 419 (1995).
12. G. Blasse, *J. Inorg. Nucl. Chem.* **27,** 2117 (1965).
13. G. Blasse, *J. Solid State Chem.* **72,** 72 (1988).